

Supporting information

Interfacial thiol-isocyanate reactions for functional nanocarriers: A facile route towards tunable morphologies and hydrophilic payload encapsulation

Sören Kuypers^{a,b}, Sumit Kumar Pramanik^{a,b}, Lien D'Olieslaeger^a, Gunter Reekmans^b, Martijn Peters^b, Jan D'Haen^{a,c}, Dirk Vanderzande^{b,c}, Tanja Junkers^{b,c}, Peter Adriaensens^{b,c} and Anitha Ethirajan^{*a,b}

^a Institute for Materials Research (IMO), Hasselt University, Wetenschapspark 1, 3590 Diepenbeek, Belgium

^b Organic and (Bio-)Polymer Chemistry, Institute for Materials Research, Hasselt University, Agoralaan D, 3590 Diepenbeek, Belgium

^c IMEC, associated lab IMOMECE, Wetenschapspark 1, 3590 Diepenbeek, Belgium
Email: anitha.ethirajan@uhasselt.be

Experimental part

Materials

All solvents were obtained from different commercial sources and further used without purification. Cyclohexane (> 99.5 %), 1,8-diazabicyclo[5.4.0]undec-7-ene (DBU) (> 99.0 %), 1,4-butanedithiol (BDT) (> 97 %), pentaerythritol tetra-3-mercaptopropionate (PETMP), toluene diisocyanate (TDI) (95 %), sodium chloride (NaCl), and doxorubicin hydrochloride (Dox.HCl) (98.0-102.0%, HPLC) were purchased from Sigma Aldrich. Potassium chloride (KCl), dimethyl sulfoxide (DMSO), Penicillin/streptomycin (P/S) and sodium dodecyl sulphate (SDS) were obtained from Merck. The surfactant Hypermer B246 (a block copolymer containing polyhydroxystearic acid and poly(ethylene glycol)) was kindly supplied by Croda Europe Ltd. Iscove's Modified Dulbecco's Medium (IMDM), Dulbecco's Modified Eagle's medium (DMEM), fetal calf serum (FCS) and alamar blue were purchased from Life Technologies. The Phosphate Buffered Saline (1xPBS) was bought at Lonza. The culture and dark plates were obtained from Greiner Bio One. HeLa cells were kindly provided by the Biophysics group of BIOMED institute (Hasselt University). Water obtained from Sartorius Stedim biotech machine was used for all the experiments.

Instrumentation

Dynamic light scattering (DLS)

The average size and size distribution of the nanocarriers were measured at 20°C by DLS using a Brookhaven instruments Zetapals.

Fourier transform infrared (FT-IR) spectroscopy

The chemical composition was analyzed using FT-IR (Bruker: Tensor 27) in transmission mode. This was done by placing few drops of miniemulsion in cyclohexane phase on a NaCl disc and letting it dry. The spectral region was analyzed from 4000 cm⁻¹ to 500 cm⁻¹.

High-resolution solid-state nuclear magnetic resonance (NMR) spectroscopy¹

For the material composition analysis, Carbon-13 solid-state CP/MAS NMR spectra were acquired on an Agilent VNMRS Direct Drive 400MHz spectrometer (9.4 T wide bore magnet) equipped with a T3HX 3.2 mm probe dedicated for small sample volumes and high decoupling powers. Magic angle spinning (MAS) was performed at 12.7 kHz with ceramic rotors of 3.2 mm in diameter (34 μl rotors). Both probe (20 l/min) and upper-barrel (30 l/min) cooling were used to limit sample heating during the experiments. The aromatic signal of hexamethylbenzene was used to determine the Hartmann-Hahn condition ($\omega_{1H} = \gamma_H B_{1H} = \gamma_C B_{1C} = \omega_{1C}$) for cross-polarization (CP), and to calibrate the carbon chemical shift scale (132.1 ppm). Acquisition parameters used were the following: a spectral width of 50 kHz, a 90° pulse length of 2.5 μs, a spin-lock field for CP of 100 kHz, a contact time for CP of 1 ms, an acquisition time of 20 ms, a recycle delay time of 15 s and 1500-3000 accumulations. High power proton dipolar decoupling during the acquisition time was set to 100 kHz.

Transmission electron microscopy (TEM)

A Tecnai Spirit TEM operating at 120 kV was used to study the morphology of the nanocarriers. The diluted samples in their respective solvents (cyclohexane for organic phase and water for aqueous phase dispersions) were drop casted and dried on TEM grids (formvar foil upon copper grids). No additional staining was done.

Synthesis:

The interfacial reaction employs following mechanism

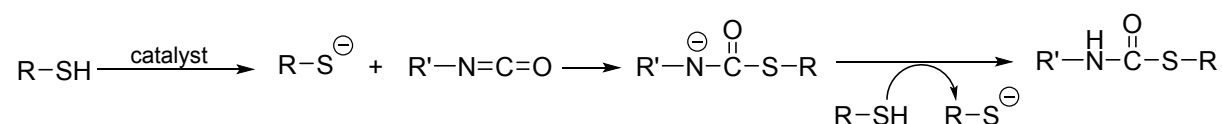


Fig. S1: A schematic representation of the reaction mechanism between a thiol and an isocyanate in the presence of base catalyst.

Preparation of nanocarriers

Two sets of reactions were done: one using catalyst and the other using elevated temperature. For all reactions the continuous phase was made by heating 10 g of cyclohexane and 200 mg of hypermer B246 at 60 °C until the surfactant was fully dissolved. An aliquot of 2.5 g was taken from the continuous phase for the additive phase. The dispersed phase contains various amounts of thiol based monomers (see Table 1), 0,35 g of 1 M KCl solution and 0.55 g DMSO. The mixture containing the continuous phase and the dispersed phase was left to pre-emulsify for 1 hour at 1000 rpm at 20 °C. Subsequently, the mixture was sonicated using a

Branson 450W digital sonifier (1/4" tip) for 3 min (30 s pulse; 20 s pause) with an amplitude of 65 %, while cooling the sample in an ice bath. An equimolar amount of TDI with respect to the thiol monomers used was added to the additive phase containing 2.5 g cyclohexane. In case of the base catalyzed reaction, the catalyst (thiol / DBU molar ratio 1: 100) was also added to the additive phase. The latter was then drop wise introduced in to the emulsion and left for stirring at room temperature in case of the base catalyzed reaction and at 60 °C overnight for reaction employing temperature. Finally, the emulsion was passed through a paper filter (Whatman, poresize 4 - 7 µm) to separate any bulk product formed from the particulate dispersion. The milky dispersions were then directly used for various characterizations.

Determination of theoretical and experimental solid content

The experimental solid content of the dispersion was determined thermogravimetrically using the formula:

$$\text{Solid Content} = \frac{\text{Net weight of dried sample}}{\text{Net weight of wet sample}} \times 100 \%$$

The theoretical solid content was determined by calculating the solid content on full conversion of all monomers added to the reaction and taking into account the weight of KCl solution and DMSO in the dispersed phase.

Redispersion of nanocapsules in water

An aqueous solution of 0.1 wt % SDS was made. 1 g of emulsion containing nanocapsules was added to 10 g of this SDS water solution and stirred at 2000 rpm for 1 hour at room temperature. This was ultrasonicated in an ultrasonication bath at 60 Hz for 5 min. After this the dispersion was left to stir overnight at 2000 rpm at room temperature. Finally the redispersed dispersion was passed through filter paper before characterization.

Analysis and characterization

All samples were treated the same way during analysis and characterization.

FT-IR analysis

First the monomers (BDT, TDI and PETMP) were analyzed to identify their characteristic peaks (Fig S2, S3, S4).

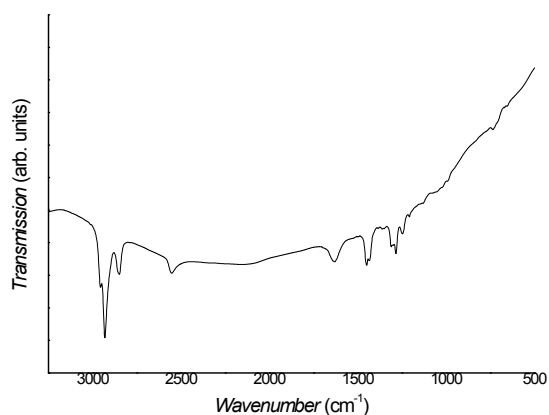


Fig. S2: FT-IR of butanedithiol monomer (BDT).

Fig S2 shows the FT-IR spectrum of BDT. The peak at 2556 cm^{-1} occurs due to the S-H vibration ($\nu(\text{S-H})$)² and the peaks at 2929 cm^{-1} and 2849 cm^{-1} due to C-H stretch of CH_2 ($\nu(\text{CH}_2)$)³.

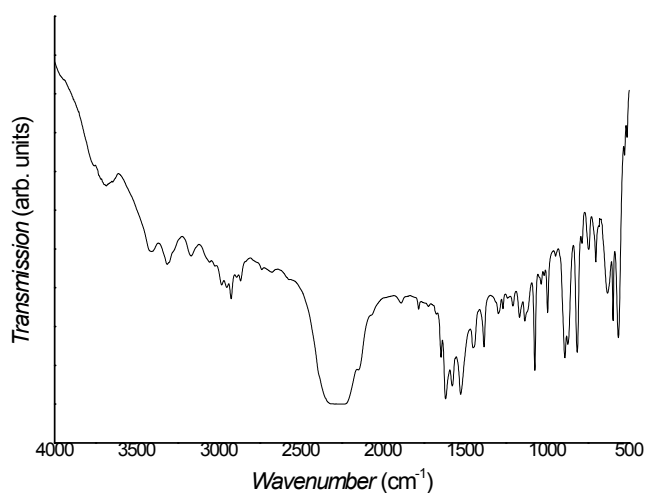


Fig. S3: FT-IR of the diisocyanate monomer, tolyene-2,4-diisocyanate (TDI).

Fig S3 shows the FT-IR spectrum of TDI, with a broad characteristic stretching vibration at $2270 - 2280\text{ cm}^{-1}$ ($\nu(\text{NCO})$)².

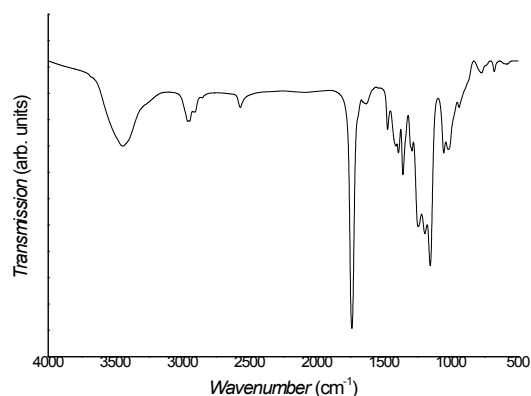


Fig. S4: FT-IR of the crosslinker, pentaerythritol tetra-3-mercaptopropionate (PETMP).

Fig S4 shows the FT-IR spectrum of PETMP. The S-H vibration of PETMP occurs at 2556 cm⁻¹ (ν (S-H)) and the peak at 1730 cm⁻¹ comes from the C=O vibration of the ester group ⁴.

A bulk reaction was done between 4 mmol BDT and 4 mmol TDI using 1/100 DBU as a catalyst to locate the characteristic thiourethane peak (Fig S5).^{5,6}

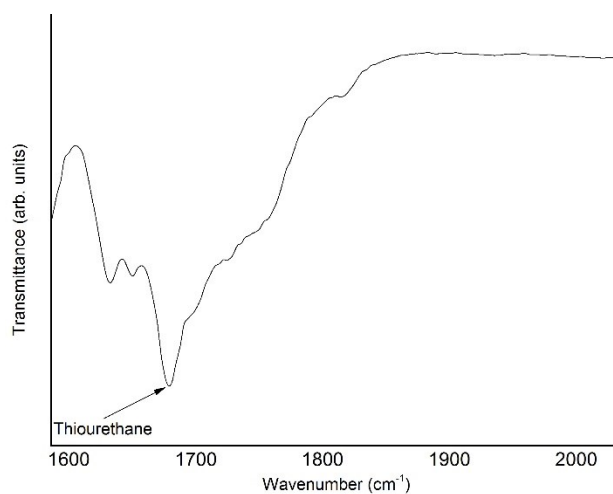


Fig. S5: Bulk reaction showing the characteristic C=O vibration of thiourethane at ~1680cm⁻¹. The spectral region ranging from 1600 cm⁻¹ to 2000 cm⁻¹ is shown here.

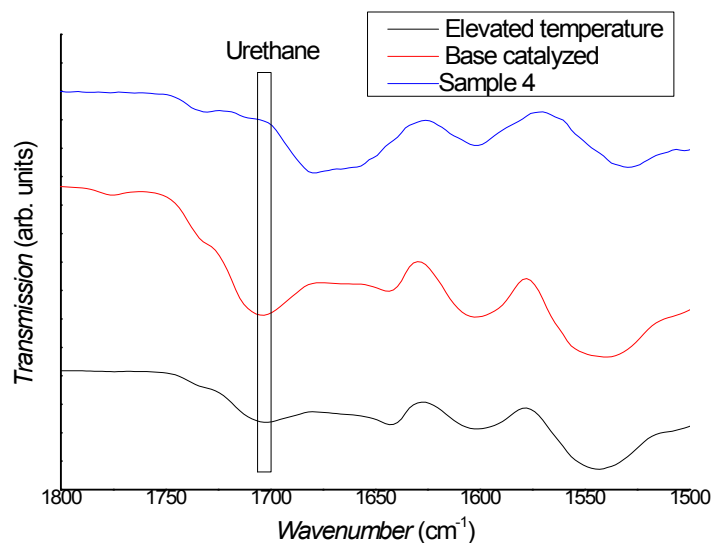


Fig. S6: FT-IR spectra showing the result of the reaction between the surfactant and TDI. The spectral region ranging from 1800 cm^{-1} to 1500 cm^{-1} is shown here.

Fig. S6 shows the result of the reaction between the surfactant and TDI using base catalyst as well as elevated temperature. For comparison, spectrum from sample 4 is also shown here. The reaction was performed in a similar way as that of the sample 4 (including the same amount of surfactant and 4 mmol diisocyanate but excluding BDT). The graph shows clearly the presence of the urethane peak ^{7,8} for the surfactant only samples (without BDT) due to the reaction of the OH functionality of the surfactant with the isocyanate used in the reaction. It is also clear that there is no defined signal for urethane at this position for sample 4 or for all the other samples (shown in Fig. S7). Though NMR shows the presence of a peak corresponding to urethane-urea, as FT-IR shows a clear presence of urea and not urethane, the peak in NMR data can therefore be attributed to the urea formation.

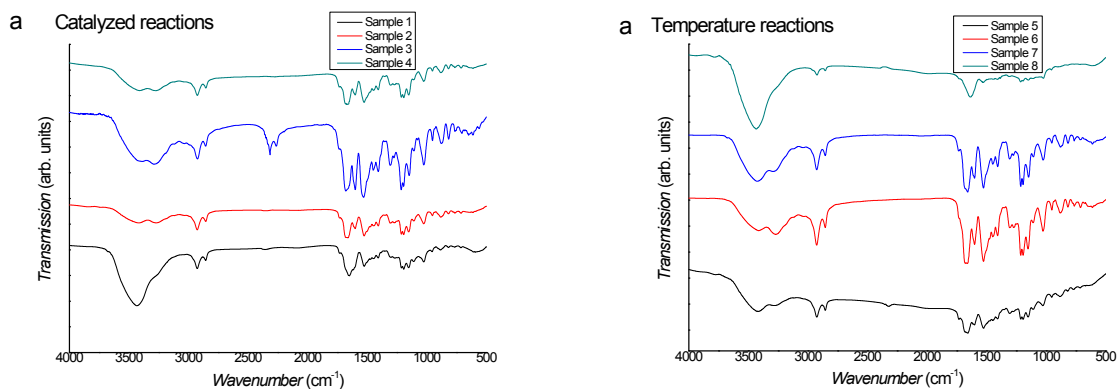


Fig. S7: a) FT-IR spectra of samples obtained by using base catalyst (a) and elevated temperature (b)

Fig. S7 (a) and (b) spectra clearly show a broad peak at 3300 cm^{-1} ($\nu(\text{O-H})$) coming from the surfactant and water, and characteristic C-H stretching vibration occurring at 2929 cm^{-1} and 2849 cm^{-1} ($\nu(\text{CH}_2)$). At $\sim 1548\text{ cm}^{-1}$ a well-defined peak can be found for ($\nu(\text{C-N})$) and ($\delta(\text{N-H})$). The peak at $\sim 1680\text{ cm}^{-1}$ indicates the presence thiourethane.^{5,6} Also a urea peak can be found at $\sim 1640\text{ cm}^{-1}$.^{7,8}

TEM characterization

The morphology of all samples was studied using TEM.

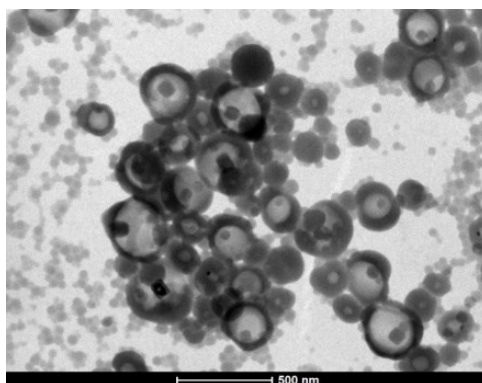


Fig. S8: TEM image obtained from sample 3 (scale bar at 500 nm). This reaction was base catalyzed and in the presence of the PETMP cross linker.

In Fig. S8, sample 3 shows that using a base catalyst and 0.1 mmol crosslinker gives a nanocapsule morphology. The core-shell structure of the nanocapsule and the presence of salt crystals encapsulated within the capsule (seen as dark spots within the capsules) are clearly visible here.

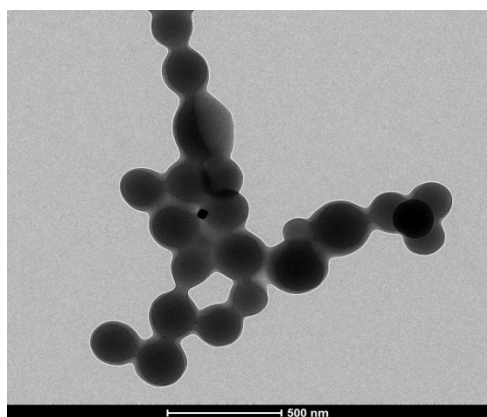


Fig S9.: TEM image obtained from sample 7 (scale bar at 500 nm). This reaction was accomplished at elevated temperature and with PETMP cross linker.

In Fig. S9, sample 7 shows that the use of elevated temperature and 0.1 mmol crosslinker gives a nanoparticle morphology in contrast to the base catalyzed reactions that yields a nanocapsule morphology.

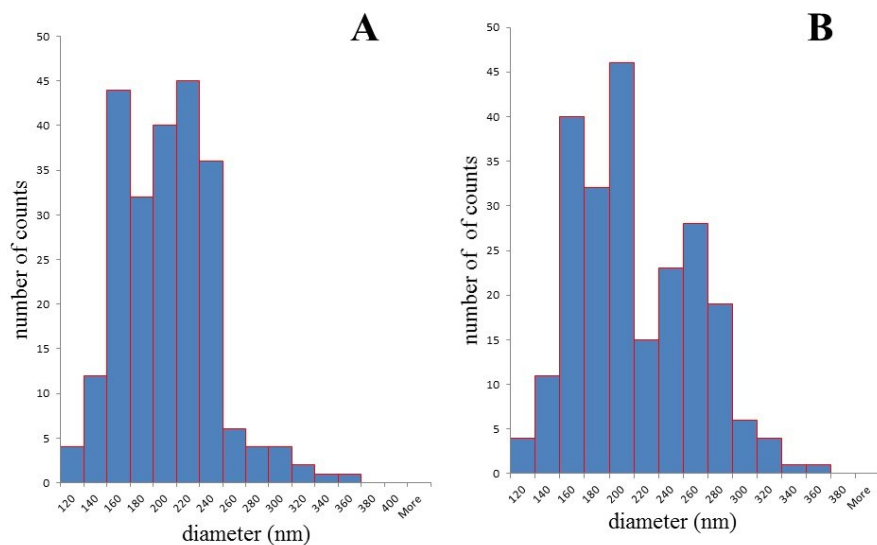


Fig S10.: Size distribution of the nanocapsules obtained from TEM images for sample 3 (A) and sample 4 (B). HClmage image processing and image analysis tools for quantitative analysis were employed . Data were obtained by measuring 231 and 214 nanocapsules for sample 3 and 4 respectively.

In Fig. S10, sample 4 shows relatively broader size distribution than that of sample 3. The average size of the nanocapsules were 202 ± 61 nm and 211 ± 86 nm for sample 3 and 4 respectively.

Energy-dispersive X-ray spectroscopy (EDX)

EDX characterization was done to determine the presence of the encapsulated salt (hydrophilic payload).

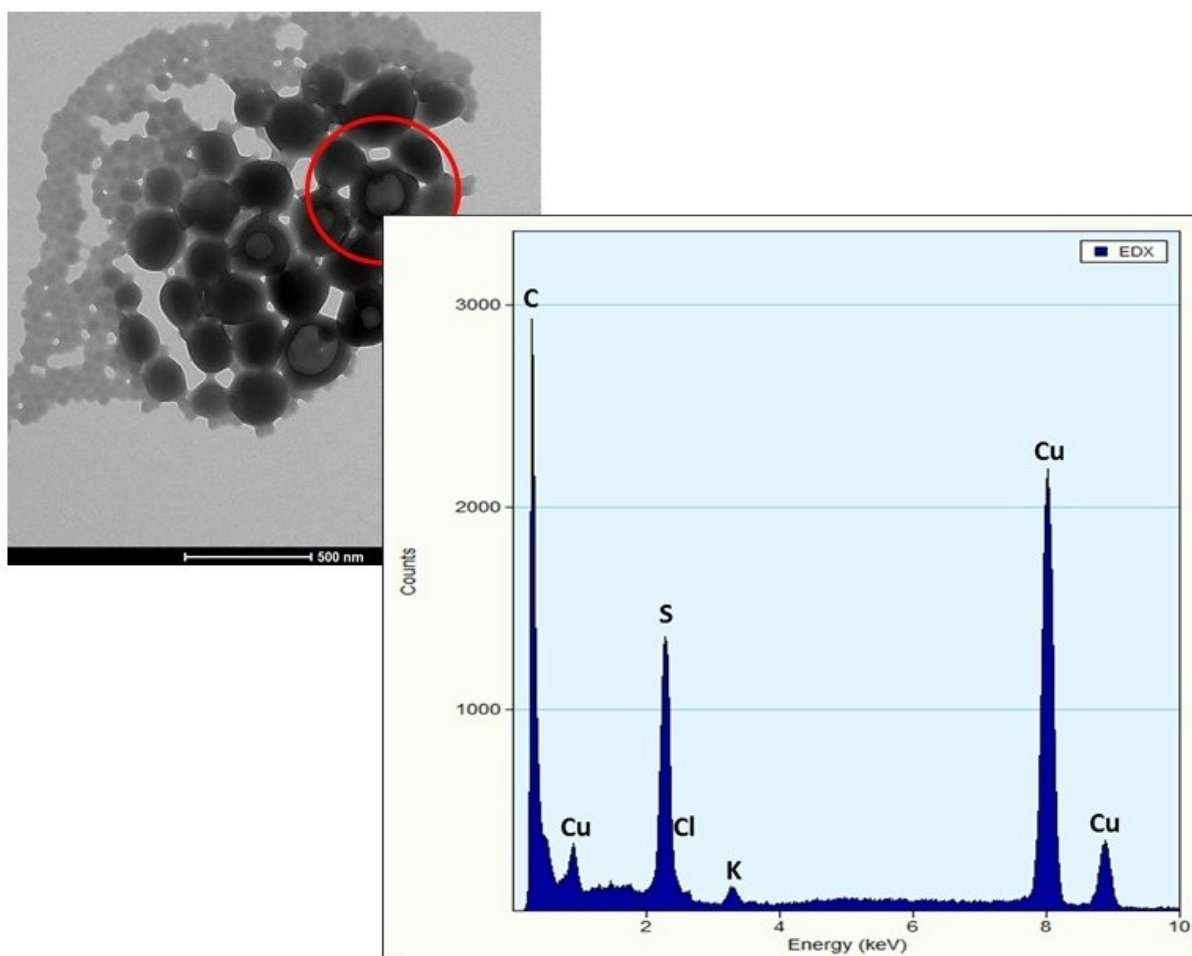


Fig. S11: EDX result for sample 4 (in organic phase) showing the presence of the hydrophilic payload KCl.

Fig S11 shows the EDX result for sample 4 in cyclohexane phase. Presence of the elements K and Cl clearly shows the successful encapsulation of the hydrophilic payload KCl. Cu signal arises from the TEM grid used for sample preparation.

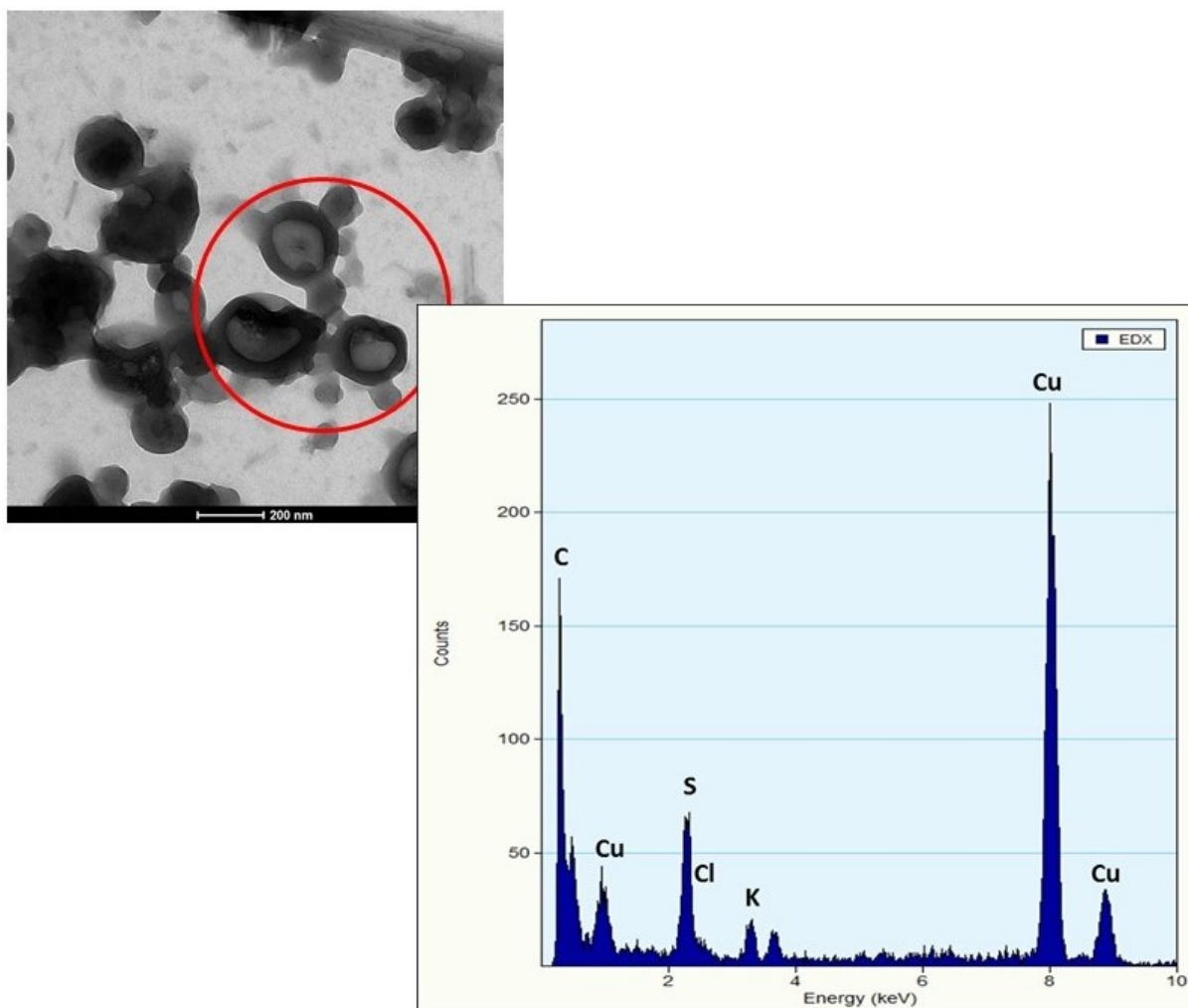


Fig. S12: result for sample 4 (in aqueous phase) showing the presence of the hydrophilic payload KCl.

Fig S12 shows the EDX result for sample 4 after redispersion in water. The presence of the elements K and Cl confirms that the shell is still intact even after redispersing the nanocarriers in water and that the salt solution has not leaked out of the nanocapsules.

With the TEM studies, it can be seen that KCl is retained within the capsules, both in cyclohexane as well as in aqueous phases. Despite that salt exists as dissolved ions within the capsule, theoretically, the diffusion to the aqueous phase due to the concentration gradient would have resulted in loss of KCl within the capsule. However, this was not the case as the salt crystals within the capsules were visible (under electron beam) in the TEM images and the presence of the elements was verified by EDX in samples after several days after redispersion in water.

Alamar blue assay.

As a proof-of-concept, the redispersed sample 3 was tested for cytotoxicity. The sample was first washed in order to remove the excess of surfactant by multiple centrifugation and redispersion (5 times). The sample was centrifuged at 10000 rpm for 20 minutes and the pellet

was redispersed with fresh deionized water. After washing, the solid content was determined thermogravimetrically. For the alamar blue assay, HeLa cells were seeded at 10 000 cells per well in a 96-well flat bottom plate together with 100 μ L of DMEM medium supplemented with 1 % P/S and 10 % FCS. The cells were left to incubate at 37 $^{\circ}$ C in a 5 % CO₂ incubator for 24 h after which they were washed with 1xPBS. A total of six wells per condition were taken and 100 μ L of the different required conditions were added to the respective wells: blank (supplemented IMDM medium), cell death (1: 9.1 dilution in supplemented IMDM medium of 1 g SDS in 10 mL MilliQ water solution), 100 μ g/mL, 50 μ g/mL and 10 μ g/mL of nanocarriers in supplemented IMDM medium. The concentration range employed were based on literature values used for cell studies using nanocapsules.^{9,10} The cells were left to incubate for 24 h in the incubator, after which they were washed 3 times with 1xPBS. Then 100 μ L of alamar blue solution, 10 % alamar blue solution in supplemented IMDM medium, was added to each well and left to incubate for another 24 h. The solution was then transferred to a dark plate and the fluorescence measured at 590 nm while exciting the solution at 570 nm using a-FLUOstar OPTIMA plate reader. The experiment was done in triplicate.

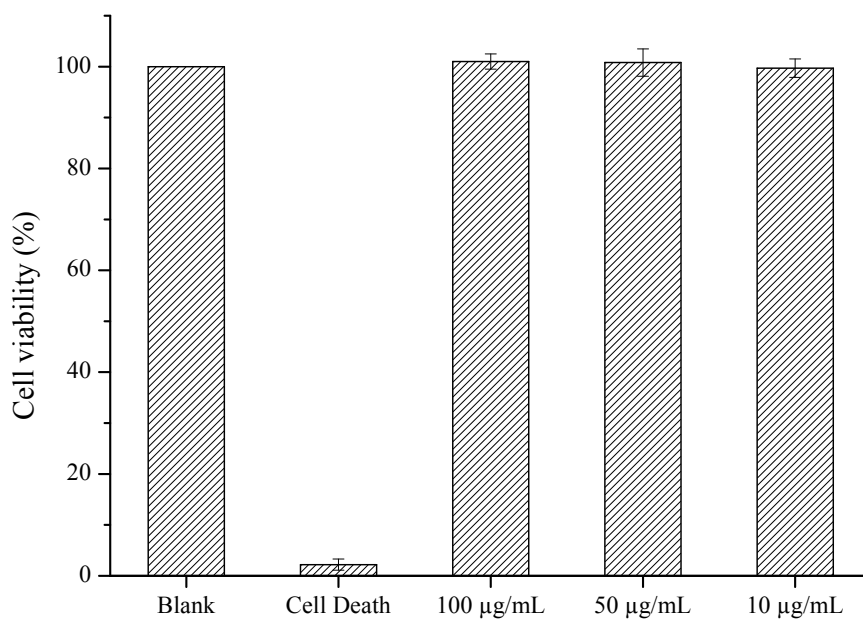


Fig. S13. Cell viability of HeLa cells after 24 h exposure to a concentration range of nanocarriers, determined using the Alamar blue assay. Data represent mean \pm standard deviation of three replicates.

Fig S13 shows that cell viability levels remained stable as compared to a control group, no decrease below 99 % was observed after exposure (24 h) to different concentrations of nanocapsules. This confirms that the synthesized nanocarriers are biocompatible. The concentrations used are notably higher than the range used in medical applications such as drug delivery, reassuring that these type of nanocarrier composition are usable for biomedical applications. One-way Anova statistical analysis was used to determine if a concentration effect was present for the sample. At $p < 0.01$ no statistically significant difference between the concentrations used was present, thereby indicating no dose-dependent effect for the used concentration range.

Encapsulation of anticancer drug

As a proof of concept doxorubicin, a potent anticancer drug, was chosen as a hydrophilic payload. The nanocapsules (NC-Dox) were prepared using the same protocol previously used for synthesizing sample 4 except for the inclusion of 1 M NaCl and 1 mg of the drug doxorubicin (Dox.HCl) instead of 1 M KCl in the formulation. The obtained dispersion (see Fig S14A) was stable without aggregates and the average size of the drug loaded nanocarriers measured using DLS was 183 nm (PDI 0.23.) The nanocapsules were redispersed in water and the leakage of the drug was studied by a method, previously reported in the literature.¹¹ As doxorubicin is a fluorescent molecule, fluorescence spectroscopy ($\lambda_{\text{ex}}=488$ nm and $\lambda_{\text{em}}=590$ nm) was used to measure the amount of free drug after redispersion in water after 24 h at 25°C. For this experiment, the redispersed nanocapsules (undialyzed) were sedimented by centrifugation at 6000 rpm for 30 min. The amount of free drug in the supernatant was compared with a reference sample. For the latter, dispersion was prepared identically using the same protocol as the drug containing nanocapsule dispersion except for the absence of the drug in the formulation. The obtained dispersion (NC-Ref) was redispersed in an aqueous SDS solution containing an equal amount of doxorubicin taken in the encapsulation experiment and then subjected to centrifugation. The amount of leaked drug and thereby the permeability of the shell of the drug loaded sample was assessed by measuring the difference in fluorescent intensities between the supernatants collected after centrifugation. All measurements were made in triplicates and an average value was taken. The fluorescence signal of the reference sample was set as 100%. From the data shown in Fig S14B, it can be seen that a small amount (about 11%) of the drug of the initially incorporated amount is detected outside of the nanocapsules in the supernatant. As the nanocapsules were subjected to mild mechanical forces during redispersion and centrifugation steps, some small damages to the nanocapsule wall leading to leakage of drug can be expected. Nevertheless, the obtained results indicates good impermeability as well as resistance of the shell towards leakage and dialysis of the samples can be done to remove any unencapsulated drugs for further biological studies.

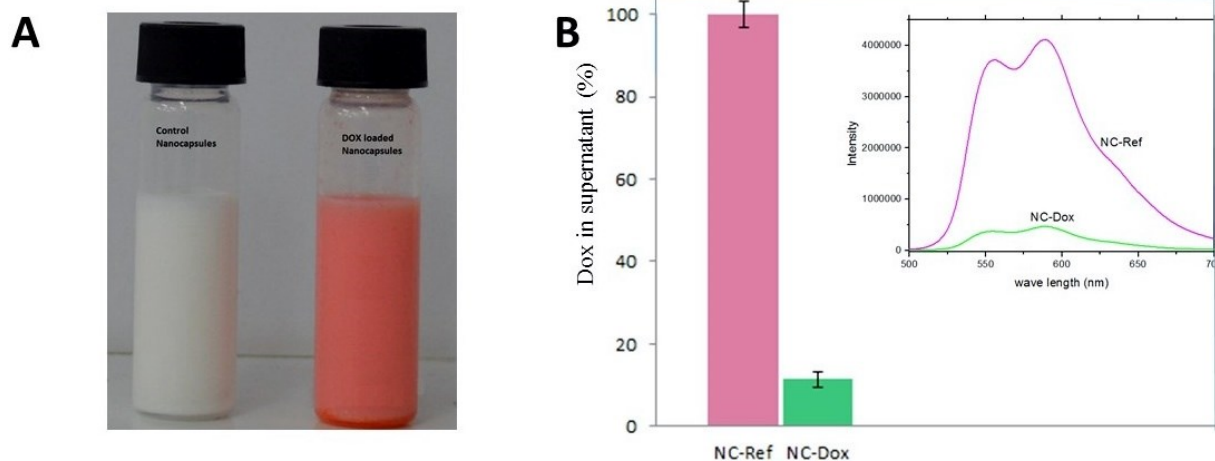


Fig. S14 (A) Stable reference (left, NC-Ref) and doxorubicin loaded (right, NC-Dox) nanocapsule dispersions. (B) Graph depicting doxorubicin leakage (Dox in supernatant %) determined by measuring the fluorescence signal of the supernatant solutions obtained from NC-Ref and NC-Dox. The corresponding steady-state emission spectra are shown in inset.

References:

1. P. Adriaensens, L. Storme, R. Carleer, J. Gelan and F. E. Du Prez, *Macromolecules*, 2002, **35**, 3965-3970.
2. J. Tan, C. Li, H. Li, H. Zhang, J. Gu, B. Zhang, H. Zhang and Q. Zhang, *Polymer Chemistry*, 2015, DOI: 10.1039/C5PY00412H.
3. S. W. Joo, S. W. Han and K. Kim, *Molecular Crystals and Liquid Crystals Science and Technology. Section A. Molecular Crystals and Liquid Crystals*, 2001, **371**, 355-358.
4. M. T. Gokmen, J. Brassinne, R. A. Prasath and F. E. Du Prez, *Chemical Communications*, 2011, **47**, 4652-4654.
5. J. F. Smith and E. C. Friedrich, *Journal of the American Chemical Society*, 1959, **81**, 161-163.
6. J. D. Flores, J. Shin, C. E. Hoyle and C. L. McCormick, *Polymer Chemistry*, 2010, **1**, 213-220.
7. U. Paiphansiri, J. Dausend, A. Musyanovych, V. Mailänder and K. Landfester, *Macromolecular Bioscience*, 2009, **9**, 575-584.
8. F. Tiarks, K. Landfester and M. Antonietti, *Journal of Polymer Science Part A: Polymer Chemistry*, 2001, **39**, 2520-2524.
9. G. Baier, S. Winzen, C. Messerschmidt, D. Frank, M. Fichter, S. Gehring, V. Mailänder and K. Landfester, *Macromolecular Bioscience*, 2015, **15**, 765-776.
10. B. Kang, P. Okwieka, S. Schöttler, O. Seifert, R. E. Kontermann, K. Pfizenmaier, A. Musyanovych, R. Meyer, M. Diken, U. Sahin, V. Mailänder, F. R. Wurm and K. Landfester, *Biomaterials*, 2015, **49**, 125-134.
11. J. M. Siebert, G. Baier, A. Musyanovych and K. Landfester, *Chemical Communications*, 2012, **48**, 5470-5472.